RP Current Trends In Applied Sciences (e-ISSN: 2583-7486)
Vol. 4, No. 2 (April – June 2025) pp. 23–30

RESEARCH PLATEAU
PUBLISHERS

Cite this article: P.M. Ganguly, A. Roy, M. Mitra, A. Chattopadhyay, DFT-based analysis of fluoride adsorption on SiO_2 surfaces: Insights into mechanisms and materials, *RP Cur. Tr. Appl. Sci.* **4** (2025) 23–30.

Original Research Article

DFT-based analysis of fluoride adsorption on SiO_2 surfaces: Insights into mechanisms and materials

Payel Mukherjee Ganguly[1,*], Arkaneell Roy[2], Mala Mitra[1], Arpita Chattopadhyay[3]

[1]Department of Physics, Sister Nivedita University, Block – DG ½, Action Area 1, Newtown, Kolkata – 700156, West Bengal, India
[2]Department of Computer Science and Engineering, Techno International New Town, Block – DG 1/1, Action Area 1, New Town, Kolkata – 700156, West Bengal, India
[3]Department of Basic Science and Humanities, Techno International New Town, Block – DG 1/1, Action Area 1, New Town, Kolkata – 700156, West Bengal, India
*Corresponding author, E-mail: payel25ganguly@gmail.com

ARTICLE HISTORY
Received: 5 April 2025
Revised: 25 June 2025
Accepted: 25 June 2025
Published: 27 June 2025

KEYWORDS
Pollution remediation;
DFT; Crystal;
Miller indices.

ABSTRACT

Fluoride pollution in our soil and water is a serious environmental and health hazard and requires effective remediation techniques. Present study analyses the adsorption technique of fluoride ions (F^-) and sodium fluoride (NaF) on SiO_2 surface using Density Functional Theory (DFT). Both super cell and non-super cell slabs of hexagonal SiO_2, with Miller indices $(1\bar{0}10)$, were explored to study adsorption behavior at the molecular level. Adsorption energies, electronic properties, and density of states were calculated for evaluating the strength of interaction between SiO_2 and fluoride adsorbates, which also reveals key features consistent with the Langmuir Isotherm model. A rightward shift in the Fermi level indicates strong electron interaction, especially by sodium fluoride, may be associated with chemical adsorption. Structural distortions and hybridization changes within the SiO_2 crystal during adsorption were further elaborated. This DFT-based study provides insights into optimizing material selection for cost-effective water treatment methods for fluoride-endemic regions.

1. Introduction

Pollution of the environment due to various contaminants creates a threat to our ecosystems and health worldwide. Particularly, the inorganic cationic and anionic pollutants significantly affect the quality of our air, water, and soil [1].

The present study focuses on the naturally occurring anionic pollutant fluoride. Fluoride is present in water as various salts like Sodium Fluoride, Sodium Fluorosilicate, Fluorosilicic acid etc. As the ionic form of fluorine, fluoride not only inhibits the initiation and progression of dental caries but also stimulates new bone formation [2]. The majority of the fluoride consumed by people comes from fluoridated water, fluoridated food and fluoridated toothpaste and other dental products [3]. Natural sources of fluorine include volcanic eruptions, forest fires, geothermal activity, and rock deposits. Minerals such as granite, basalt, limestone, sandstone, volcanic rock, and coal ash also contribute to the natural occurrence of fluorine. Additionally, industrial activities—such as those in the aluminium and zinc industries, magnesium smelting, coal burning, oil refining, ceramic, glass and enamel manufacturing, and clay burning—are responsible for fluoride emissions into the environment [4]. The semiconductor industry also generates fluoride-contaminated waste water [5].

The maximum permissible limit of fluoride in drinking water is 1.5 ppm, as per specifications by WHO [6] and Indian standard [7]. However, fluoride concentrations above this limit can cause dental fluorosis, which is characterized by yellowish or brownish mottling of the tooth surface. In addition, higher fluoride levels can lead to skeletal fluorosis as well, which may lead to skeletal decay, osteoporosis, osteosarcoma, neurological defects, muscle wasting, paralysis [4]. Fluoride can also affect kidney function, liver-specific enzymes, cell morphology, and the immune system by damaging cellular genetic material [4]. Moreover, adverse effects on plants have been observed through soil and water exposure [8].

For many decades, alum was a popular choice for removing fluoride from water [9-11]. More recent studies have expanded on this approach. For example, polymeric aluminium-modified activated carbon has been used for fluoride removal from coal mining water [12]. Another study used one-step hydrothermal technique involving Mg/Fe/La hydrotalcite-like compound for fluoride adsorption in aqueous solutions [13]. Various adsorbents like diatomite, calcium bentonite, bamboo charcoal, and rice husk biochar have also been applied for the removal of fluoride from water [14]. Some studies also calculated the scope of fluoride remediation using 3D porous rhombohedral Fe-modified MgO [15], calcite permeable reactive barrier [16], on intrinsic B-doped and Al-doped graphene [17]. In computational studies, researchers primarily utilize methods such as Ab Initio Molecular Dynamics (AIMD) simulations [17], Density Functional theory (DFT) [15], Monte Carlo Simulations [18, 19], Hartree-Fockapproach [20, 21].

The present study adopts a theoretical approach to select suitable material for fluoride remediation via adsorption using

DFT [22] with silicon dioxide (SiO_2.) as the chosen adsorbent. DFT has become an indispensable tool for studying pollutant removal at the molecular and atomic levels. By analyzing adsorption, electronic properties, charge transfer, and energy landscapes, DFT provides deep insights into how pollutants interact with various materials. The adsorption energy, a key parameter calculated using DFT, determines the strength of pollutant binding on a surface; a negative adsorption energy indicates an exothermic and stable process. Essentially, DFT approximates the exchange-correlation energy that governs electron–electron interactions.

Material selection is crucial for the pollutant remediation techniques. SiO_2 is selected in the present study, due to its high surface area, tunable pore size, and versatile surface chemistry. SiO_2, the primary constituent of sand, is chosen as the adsorbent material because of its low cost, straightforward design, ease of use, and reduced production of hazardous byproducts. The term adsorption method here refers to a phase separation process used to filter water, whereby contaminants (or adsorbate) are transferred from the liquid phase to the surface or interface of the adsorbent [23]. Since experimental methods for adsorbent synthesis can be resource-intensive, DFT allows for the virtual screening of SiO_2 (or any other suitable composite) to prioritize promising candidates, thereby reducing material waste and R&D expenses. This strategy aligns with global needs for affordable water treatment solutions, particularly in fluoride-endemic regions.

In the present study, the pollutant is considered both in the form of the fluoride ion and as sodium fluoride (NaF). The adsorption energy of the SiO_2 slab was calculated before and after the adsorption of the fluoride ion and sodium fluoride; negative energy values indicate an exothermic and thermodynamically favourable process. This suggests a strong binding affinity of both fluoride and sodium fluoride to the SiO_2 surface, reinforcing its potential as an effective adsorbent. It is important to note that the accuracy of these adsorption energy calculations is highly dependent on the choice of the exchange-correlation functional within DFT [24].

2. Materials and methods

As mentioned earlier, for the analysis of the adsorption process of fluoride/NaF on silica surface, DFT was employed in the current study. For the exchange-correlation functional, the local-density approximation (LDA) [25] with ultra-soft pseudopotentials (USPP) [26] was used to study the adsorption energy of the SiO_2 hexagonal crystal [27].

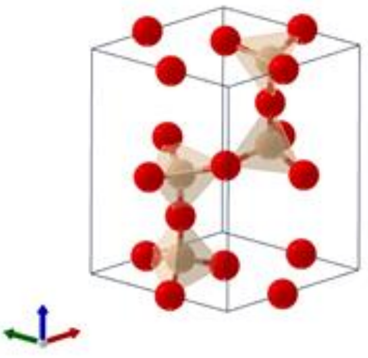

Figure 1: SiO_2 (silica) hexagonal ($P6_322$) beta-tridymite structure.

To analyse the surface properties, slab with miller indices $(10\bar{1}0)$ was generated using the python package, pymatgen [28]. SiO_2 crystallizes in the hexagonal P6-22 space group and exhibits a beta-tridymite structure [29]. In this structure, SiO_2 tetrahedra, which share corners, are formed when Si^{4+} is coordinated to four O^2 atoms. The tetrahedra structure features Si–O bonds with bond length 1.62 Å. Furthermore, the two O^{2-} sites are inequivalent, at the first O^{2-} site, two similar Si^{4+} atoms are arranged in a linear geometry, while at the second site, two analogous Si^{4+} atoms (as derived from the Materials Project database) are linked to oxygen in a bent geometry with an angle of approximately 150°.

The surface convergence energy of SiO_2 was determined by optimizing the atomic positions at different adsorption sites and through the adjustment of structural parameters. The cut off energy was set at 40 Ry for the wave function and 320 Ry for the charge density with k-point mesh of Γ−sampling points. For ion dynamics, the Broyden–Fletcher–Goldfarb–Shanno (BFGS) algorithm was employed for geometry relaxation, given its efficiency as a quasi-Newton optimization method.

The adsorption energy (E_{ads}) of SiO_2 quantifies the energetic change that occurs when a pollutant adheres to an adsorbent surface [30].

$$E_{ads} = E_{sys} - [E_{surface} + E_{pollutant}]$$

where, E_{sys} is the total energy of the combined system, which includes the adsorbent surface with the pollutant already adsorbed, $E_{surface}$ is the energy of the clean, unmodified adsorbent surface and $E_{pollutant}$ is the energy of the isolated pollutant before it interacts with the surface.

All calculations were performed using the Quantum ESPRESSO computational package. The energy cutoff was chosen based on a convergence study, as shown in Figure 2.

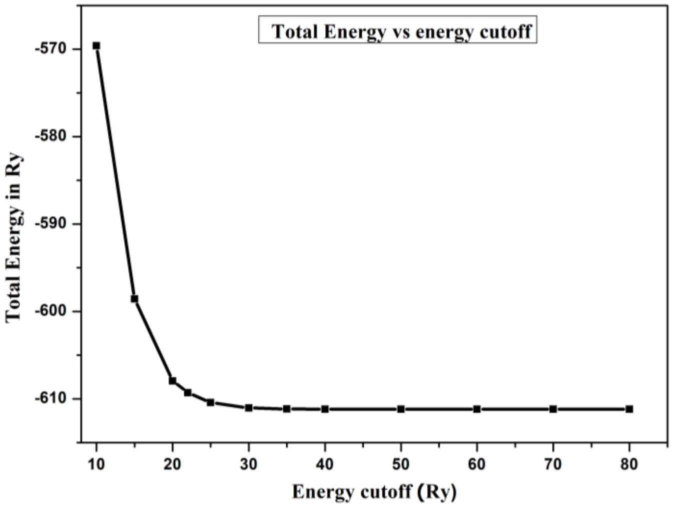

Figure 2: Total energy vs. the energy cut-off.

3. Results and discussion

This section focuses on the structural and electronic properties under study through Density Functional Theory.

In Figure 3(a), we present the slab structure of SiO_2, as obtained from the Materials Project. A suitable plane corresponding to Miller indices $(10\bar{1}0)$ was cut using a Python module. Although the hexagonal structure employs Bravais Miller indices, we have converted them into equivalent threecoordinate indices, as rotational effects will not be studied. Figure 3(b) shows the twelve adsorption sites for fluoride ions on the surface of SiO_2. These adsorption sites were identified using a python package [31]. Figure 3(c) illustrates the formation of the supercell structure of SiO_2, while Figure 3(d) depicts the presence of thirty fluoride adsorption sites on the supercell structure.

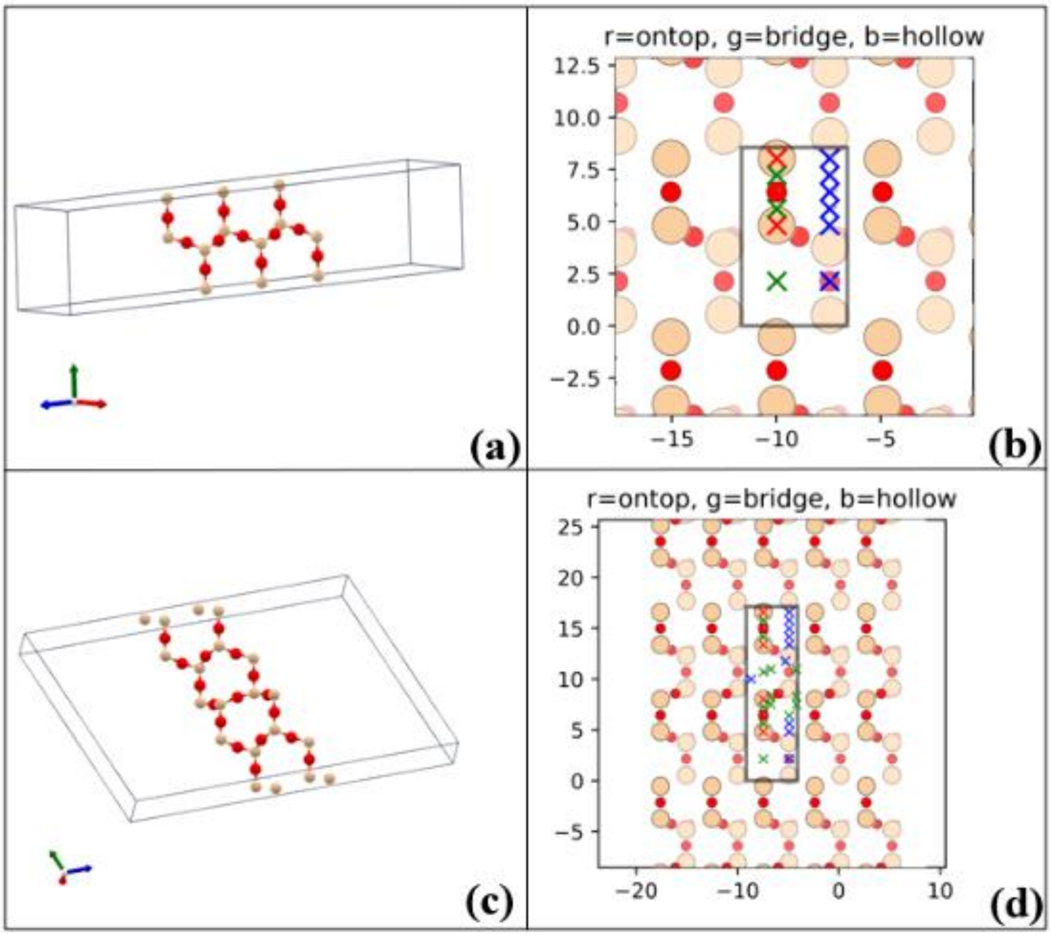

Figure 3: (a) Hexagonal crystal structure of SiO_2; (b) fluoride adsorption sites on SiO_2; (c) supercell structure of above SiO_2 crystal; (d) fluoride adsorption sites in the supercell.

3.1 Adsorption energy calculation

We calculated the adsorption energy for each adsorption site identified on both the SiO_2 crystal plane $(10\bar{1}0)$ and the same plane within the supercell structure. Separate calculations were conducted for sodium fluoride (NaF) and the fluoride ion (F^-). The results, shown in the accompanying table, indicate that all calculated adsorption energy values are negative. These negative values confirm that the adsorption process is exothermic, signifying that the adsorption of both NaF and fluoride ions onto the SiO_2 surface is thermodynamically favourable.

Table 1: Calculation of Adsorption energy for the adsorption sites of SiO_2 crystal unit cell and supercell both for adsorbate NaF and Fluoride ion.

Crystal structure	**Adsorbent energy(Ry)**	**Adsorbate energy (Ry)**	**combined energy(Ry)**	**Adsorption energy(Ry)**
	SiO_2	**NaF**	**NaF+SiO_2**	
SiO_2	-471.62	-143.76	-615.55	-0.17
	-471.62	-143.76	-615.61	-0.23
SiO_2 Supercell	-704.73	-143.76	-848.63	-0.13
	-704.73	-143.76	-848.62	-0.12
Crystal structure	**Adsorbent energy(Ry)**	**Adsorbate energy (Ry)**	**combined energy(Ry)**	**Adsorption energy(Ry)**
	SiO_2	**F^-**	**F^- + SiO_2**	
SiO_2	-471.62	-48.60	-520.56	-0.34
	-471.62	-48.60	-520.42	-0.19
SiO_2 Supercell	-703.92	-48.60	-753.35	-0.83
	-703.92	-48.60	-753.34	-0.82

3.2 Electronic properties

The study of electronic properties on the hexagonal crystal of SiO_2 were done. For different adsorbates like the sodium fluoride and fluoride ion on both supercell and non-supercell slab of the SiO_2 crystal shown in Figure 4.

In Figure 4(a) and Figure 4(c), the shift of fermi level accounted from -1.453 eV to 1.056 eV. This heavy rightward shift of the fermi level indicates the high electron donation of sodium fluoride towards the SiO_2 slab. Similarly in Figure 4(b) and Figure 4(d), the fermi level shifted from -1.453 eV to 0.273 eV which indicates the similar trend like sodium fluoride, but the effect is notably weaker than sodium fluoride.

It is noticed that the peak density of states was observed in the range of approximately around –7.5 eV to 5 eV near the fermi level. In Figure 4(a), (b), (c), (d), after the 10th adsorption, the number of states increases suddenly.

This progressive shift of the fermi level indicates a strong atomic interaction between the SiO_2 surface and the adsorbate which is a characteristics of chemisorptions [32]. In case of physisorption, the interaction between adsorbate and adsorbent is very weak, which can show a less progressive change in the fermi level.

For individual adsorbate, the change of the electronic properties were also analyzed.

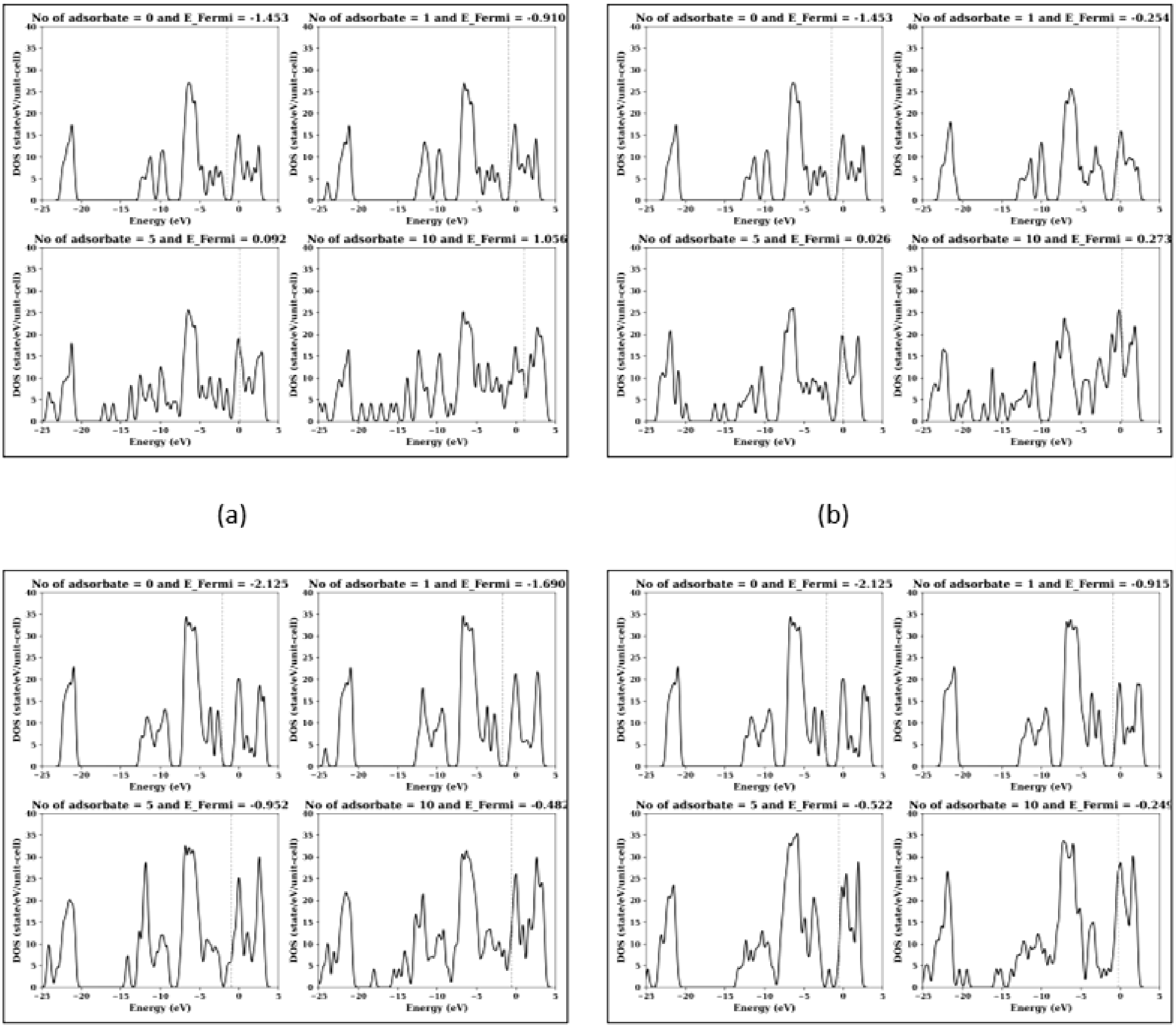

(a)

(b)

(c)

(d)

Figure 4: Variation of density of states with energy with increasing number of adsorbate: (a) SiO_2 with NaF adsorbate; (b) SiO_2 with fluoride ion adsorbate; (c) SiO_2 (supercell) with NaF adsorbate; (d) SiO_2 (supercell) with fluoride ion adsorbate.

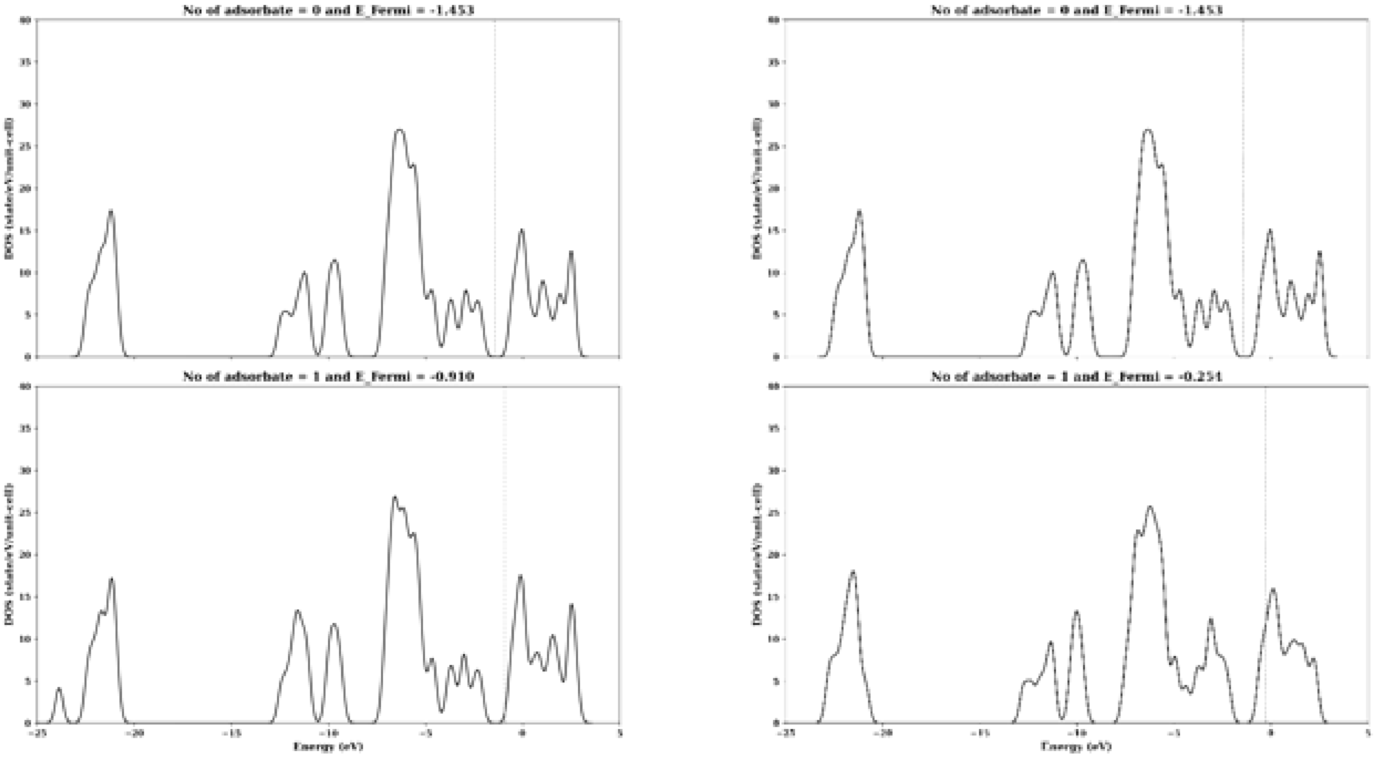

Figure 4: (e) SiO_2 with single NaF adsorbate; (f) SiO_2 with single fluoride ion adsorbate.

The energy difference observed from Figure 4(e) and (f) is about -0.656 eV which indicates the strong electronic interaction of the sodium fluoride over fluoride ion.

Adsorption also alters the hybridization of the crystal, as detected through the density of states (DOS). The SiO_2 has a hybridization is sp_3 [33] which forms a tetrahedral structure. After adsorption the tetrahedral shape get distorted in terms of Si-O bond lengths (before adsorption:1.61Å , after adsorption:1.66 Å) and angles (before adsorption:150^o , after adsorption: 112^o) on the surface because of the formation of new bond with silicone in SiO_2 with the adsorbate which is clearly visible from the DOS.

The localization of the negative charge is clearly visible from the DOS, as the fermi level shifts progressively along with accumulation of the negative charge on the surface. From the Fermi-Dirac distribution of the adsorption [34] is also give the proper accumulation of the electrons from adsorbate on the surface of SiO_2 adsorbent.

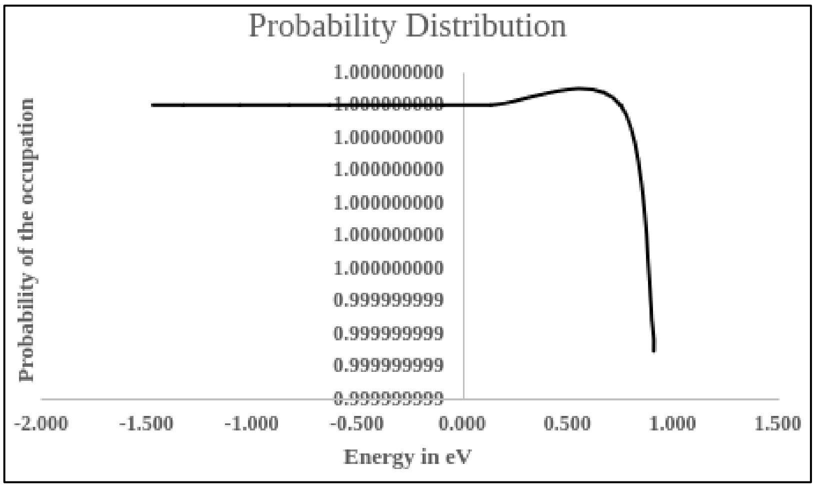

Figure 5: Fermi-Dirac Distribution of the adsorption process.

Langmuir Isotherm

One widely accepted model for explaining how molecules adsorb onto a solid surface is the Langmuir Isotherm (LI). Density Functional Theory (DFT) simulations, along with other computational and experimental adsorption investigations greatly benefit from its application. By providing molecular-level insights into adsorption processes, DFT can complement Langmuir parameters, even though the Langmuir Isotherm is typically derived from experimental data.

Using xcrysden [35], Figure 6, is showing how the adsorbate is being attached in the surface of adsorbent with increasing concentration of adsorbate.

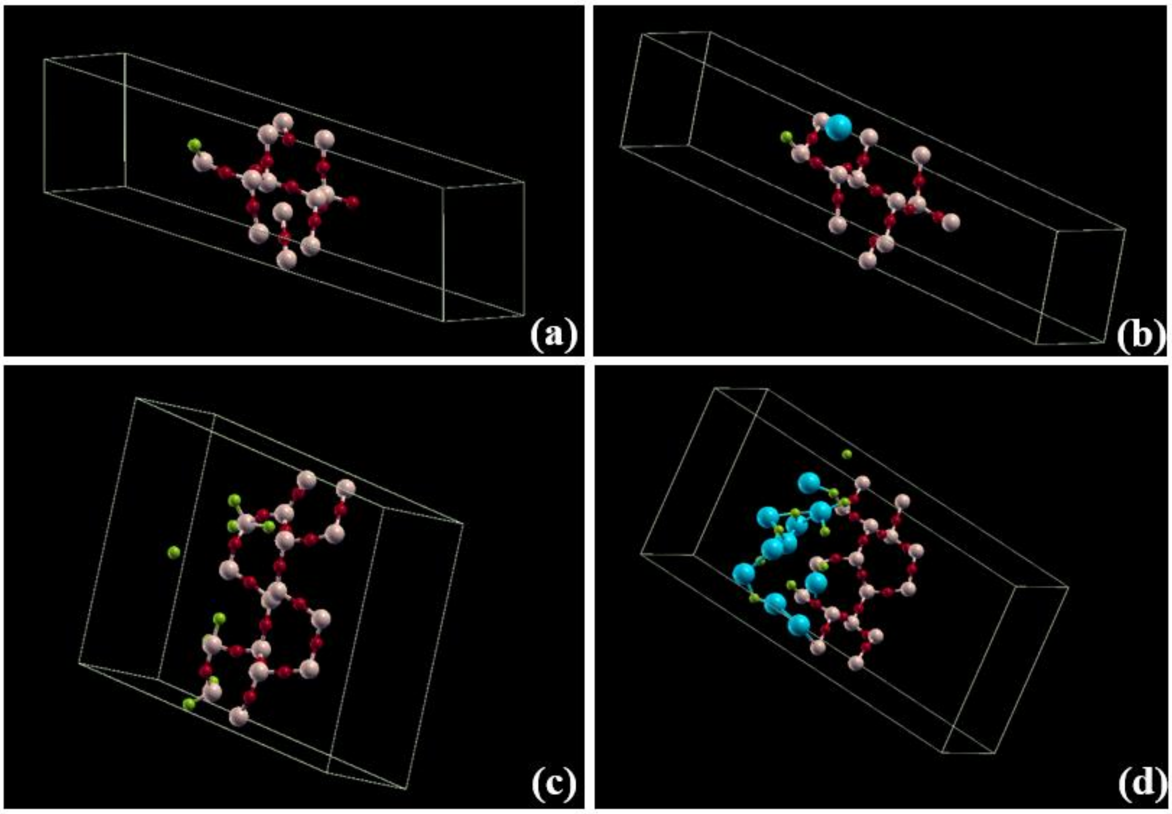

Figure 6: (a) $SiO_2$with single Fluoride ion as adsorbate; (b) $SiO_2$with single sodium fluoride (NaF) molecule as adsorbate; (c) SiO_2 supercell with 10 number of Fluoride ions as adsorbate; (d) SiO_2supercell with 10 sodium fluoride (NaF) molecules as adsorbate.

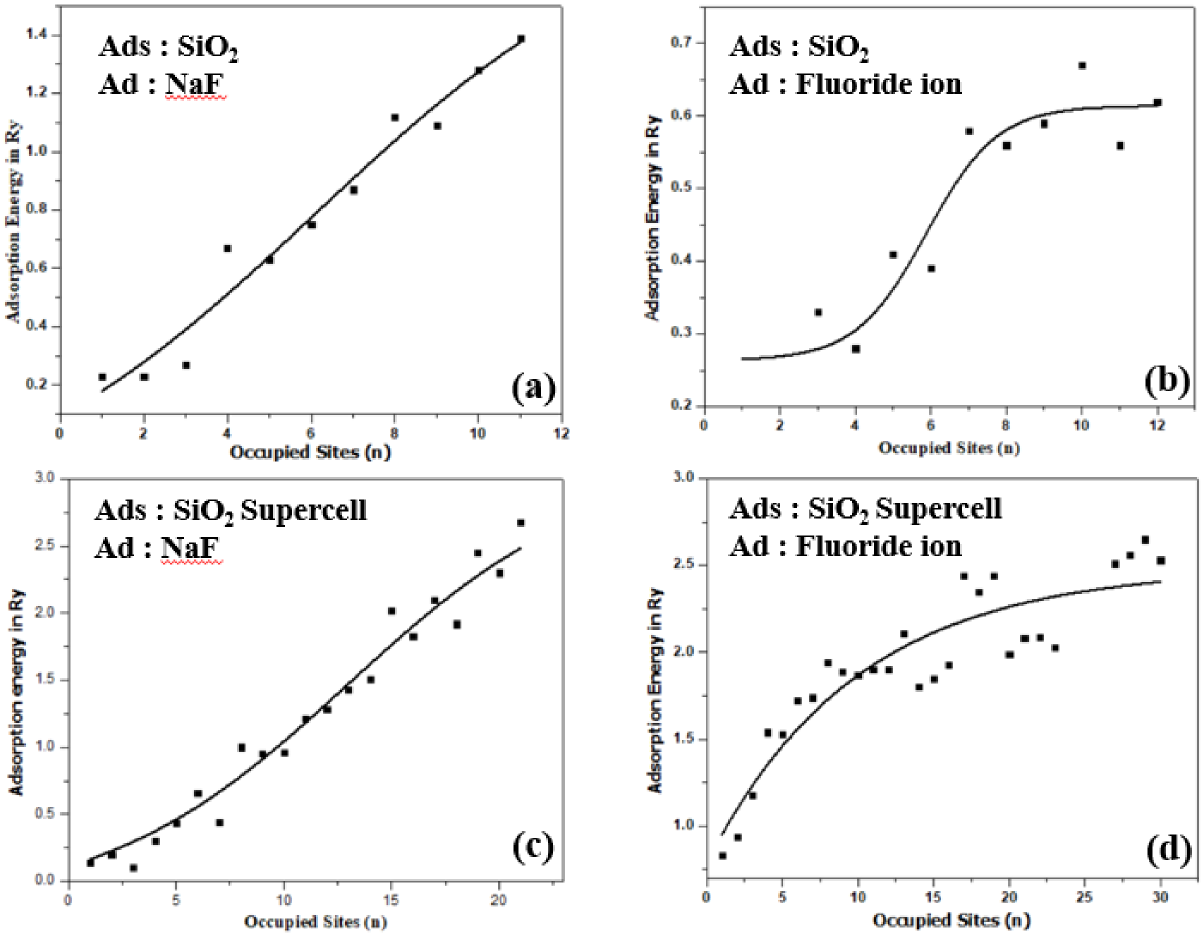

Figure 7: Variation of adsorption energy with increasing concentration of adsorbate (Ad) in the adsorbent (Ads), curves are being calibrated with Boltzman polynomial curve fitting Equation: $Y = A_2 + (A_1 - A_2)/(1+\exp((x-x_0)/dx))$. (a) adsorbent is SiO_2, adsorbate NaF; (b) adsorbent is SiO_2, adsorbate fluoride ion; (c) adsorbent is SiO_2 supercell, adsorbate NaF; (d) adsorbent is SiO_2 supercell, adsorbate fluoride ion.

LI predicts the isotherm behaviour for varying fluoride concentration. In this study, we gradually increased the concentrations of sodium fluoride (NaF) and fluoride ions (F^-) at each site depicted in Figure 3(b) and Figure 3(d). The results show in Figure 7 that the adsorption energy initially increases with the higher fluoride concentrations. However, after some time, the energy saturates as the adsorption sites become fully occupied and can no longer accommodate additional adsorbate ion/molecule. This characteristic behaviour of the graph aligns with the predictions of the Langmuir Isotherm (LI) [36, 37].

4. Conclusions

The present study demonstrates the role of SiO_2 as a promising adsorbent for fluoride remediation, using DFT-based analysis. The chemical interactions between the SiO_2 surface and fluoride adsorbates (NaF and F^-) are confirmed byhigh adsorption energy values, Fermi level shifts, and changes in electronic properties. Furthermore, the adsorption behavior was validated by the Langmuir Isotherm model which shows its efficiency and saturation characteristics. These findings provide a computational modelling for optimizing material design and cost-effective, sustainable water treatment solutions.

Acknowledgements

Our sincere thanks are extended to CDAC, Pune's supercomputing resources on PARAM KAMRUPA.

Authors' contributions

The author read and approved the final manuscript.

Conflicts of interest

The author declares no conflict of interest.

Funding

This research received no external funding.

Data availability

No new data were created.

References

[1] S.R.J. Oliver, Cationic inorganic materials for anionic pollutant trapping and catalysis, *Chem. Soc. Rev.* **38** (2009) 1868-1881.

[2] G. Das, V. Tirth, S. Arora, A. Algahtani, M. Kafeel, A.H.G. Alqarni, P. Saluja, H. Vij, S.S. Bavabeedu, A. Tirth, Effect of fluoride concentration in drinking water on dental fluorosis in southwest Saudi Arabia, *Int. J. Environ. Res. Public Health* **17** (2020) 3914.

[3] *Fluoride in Drinking Water: A Scientific Review of EPA's Standards*, National Academies Press, Washington, D.C. (2006).

[4] H. Kabir, A.K. Gupta, S. Tripathy, Fluoride and human health: Systematic appraisal of sources, exposures, metabolism, and toxicity, *Crit. Rev. Environ. Sci. Technol.* **50** (2020) 1116–1193.

[5] Y. Qiu, L.-F. Ren, L. Xia, J. Shao, Y. Zhao, B. Van der Bruggen, Hazardous fluoride and silica removal from semiconductor wastewater in a waste control by waste principle, *Social Science Research Network, Rochester, NY* (2022) 4009571.

[6] S. Ali, S.K. Thakur, A. Sarkar, S. Shekhar, Worldwide contamination of water by fluoride, *Environ. Chem. Lett.* **14** (2016) 291–315.

[7] B. Bera, S. Bhattacharjee, M. Chamling, A. Ghosh, N. Sengutpa, S. Ghosh, High fluoride in groundwater and fluorosis related health hazard in Rarh Bengal, India: a socio-environmental study, *Curr. Sci*. **120** (2021) 1225.

[8] K. Kumar, A. Giri, P. Vivek, T. Kalaiyarasan, B. Kumar, Effects of fluoride on respiration and photosynthesis in plants: An overview, *Annals Environ. Sci. Toxic*. **2** (2017) 43-47.

[9] S. Dubey, M. Agarwal, A.B. Gupta, Experimental investigation of Al-F species formation and transformation during coagulation for fluoride removal using alum and PACl, *J. Mol. Liq*. **266** (2018) 349-360.

[10] M.G. Sujana, R.S. Thakur, S.B. Rao, Removal of fluoride from aqueous solution by using alum sludge, *J. Coll. Inter. Sci*. **206** (1998) 94-101.

[11] W. Nigussie, F. Zewge, B.S. Chandravanshi, Removal of excess fluoride from water using waste residue from alum manufacturing process, *J. Hazar. Mater*. **147** (2007) 954-963.

[12] Y. Bao, Y. Qi, Q. Li, L. Wang, Z. Cao, J. Li, M. Wu, J. Chen, H. Zhang, Q. Guo, B. Jiang, J. Zhong, J. Li, Fluoride removal from coal mining water using novel polymeric aluminum modified activated carbon prepared through mechanochemical process, *J. Environ. Sci*. **146** (2024) 226-236.

[13] P. Wu, J. Wu, L. Xia, Y. Liu, L. Xu, S. Song, Adsorption of fluoride at the interface of water with calcined magnesium–ferri–lanthanum hydrotalcite-like compound, *RSC Adv*. **7** (2017) 26104-26112.

[14] J. Tang, B. Xiang, Y. Li, T. Tan, Y. Zhu, Adsorption characteristics and charge transfer kinetics of fluoride in water by different adsorbents, *Front. Chem.* **10** (2022) 917511.

[15] X. Wang, J. Wei, W. Peng, J. Dan, J. Wang, J. Zhang, Evaluation and DFT analysis of 3D porous rhombohedral Fe-modified MgO for removing fluoride efficiently, *Appl. Surf. Sci*. **552** (2021) 149423.

[16] Q. Cai, B.D. Turner, D. Sheng, S. Sloan, Application of kinetic models to the design of a calcite permeable reactive barrier (PRB) for fluoride remediation, *Water Res*. **130** (2018) 300-311.

[17] T. Chen, L. An, X. Jia, A DFT-based analysis of adsorption properties of fluoride anion on intrinsic, B-doped, and Al-doped graphene, *J. Mol. Model* **27** (2021) 56.

[18] E.V. Albano, K. Binder, D.W. Heermann, W. Paul, Adsorption on stepped surfaces: A Monte Carlo simulation, *Surf. Sci*. **223** (1989) 151-178.

[19] E. Ustinov, Kinetic Monte Carlo approach for molecular modeling of adsorption, *Curr. Opin. Chem. Eng*. **24** (2019) 1-11.

[20] T.B. Grimley C. Pisani, Chemisorption theory in the Hartree-Fock approximation, *J. Phys. C: Solid State Phys*. **7** (1974) 2831.

[21] E. Vessally, S. Soleimani-Amiri, A. Hosseinian, L. Edjlali, A. Bekhradnia, The Hartree-Fock exchange effect on the CO adsorption by the boron nitride nanocage, *Physica E: Low-dimen. Syst. Nanostr*. **87** (2017) 308–311.

[22] Mandeep, A. Gulati, R. Kakkar, Graphene-based adsorbents for water remediation by removal of organic pollutants: Theoretical and experimental insights, *Chem. Eng. Res. Design* **153** (2020) 21-36.

[23] F. Cheng, J. Wang, Removal of bisphenol a from wastewater by adsorption and membrane separation: Performances and mechanisms, *Chem. Eng. J*. **484** (2024) 149414.

[24] M.A.L. Marques, M.J.T. Oliveira, T. Burnus, Libxc: A library of exchange and correlation functionals for density functional theory, *Comp. Phys. Commun.* **183** (2012) 2272-2281.

[25] J. Toulouse, F. Colonna, A. Savin, Short-range exchange and correlation energy density functionals: Beyond the local-density approximation, *The J. Chem. Phys*. **122** (2004) 014110.

[26] B. Walker, R. Gebauer, Ultrasoft pseudopotentials in time-dependent density-functional theory, *The J. Chem. Phys*. **127** (2007) 164106.

[27] K. Mathew, A.K. Singh, J.J. Gabriel, K. Choudhary, S.B. Sinnott, A.V. Davydov, F. Tavazza, R.G. Hennig, "MPInterfaces: A Materials Project based Python tool for high-throughput computational screening of interfacial systems, *Comput. Mater. Sci*. **122** (2016) 183-190.

[28] S.P. Ong, W.D. Richards, A. Jain, G. Hautier, M. Kocher, S. Cholia, D. Gunter, V.L. Chevrier, K.A. Persson, G. Ceder,

Python Materials Genomics (pymatgen): A robust, open-source python library for materials analysis, *Comput. Mater. Sci.* **68** (2013) 314-319.

[29] A preliminary study of the crystal structure of low tridymite - Society of Glass Technology. Accessed: Apr. 05, 2025. Online available: https://sgt.org/store/viewproduct.aspx?id=17428917

[30] X. Wei, C. Dong, Z. Chen, K. Xiao, X. Li, A DFT study of the adsorption of O_2 and H_2O on Al(111) surfaces, *RSC Adv.* **6** (2016) 56303-56312.

[31] E. Pedretti, P. Restuccia, M.C. Righi, Xsorb: A software for identifying the most stable adsorption configuration and energy of a molecule on a crystal surface, *Comp. Phys. Commun.* **291** (2023) 108827.

[32] Density Functional Theory study of the adsorption of oxygen and hydrogen on 3d transition metal surfaces with varying magnetic ordering, *ResearchGate* (2024). Accessed: Apr. 05, 2025. Online available: https://www.researchgate.net/publication/356445028_Density_Functional_Theory_Study_of_the_Adsorption_of_Oxygen_and_Hydrogen_on_3d_Transition_Metal_Surfaces_with_Varying_Magnetic_Ordering

[33] N. Lopez, F. Illas, G. Pacchioni, Adsorption of Cu, Pd, and Cs atoms on regular and defect sites of the SiO_2 surface, *J. Am. Chem. Soc.* **121** (1999) 813-821.

[34] S.-J. Park, J.-B. Donnet, Evaluation of the distribution function of adsorption site energies based on the Fermi–Dirac's Law in a monolayer, *J. Colloid Inter. Sci.* **200** (1998) 46-51.

[35] M.J. Rutter, C_2x: A tool for visualisation and input preparation for Castep and other electronic structure codes, *Comp. Phys. Commun.* **225** (2018) 174-179.

[36] Patiha, E. Heraldy, Y. Hidayat, M. Firdaus, The langmuir isotherm adsorption equation: The monolayer approach, *IOP Conf. Ser.: Mater. Sci. Eng.* **107** (2016) 012067.

[37] S.R. Olsen, F.S. Watanabe, A method to determine a phosphorus adsorption maximum of soils as measured by the Langmuir isotherm, *Soil Sci. Soc. Am. J.* **21** (1957) 144-149.